BWR Pipe Crack and Weld Clad Overlay Studies*

by

W. J. Shack, T. F. Kassner, P. S. Maiya,
J. Y. Park and W. E. Ruther

Materials Science and Technology Division
ARGONNE NATIONAL LABORATORY
Argonne, Illinois

and

E. F. Rybicki

E. F. Rybicki, Inc.
Tulsa, Oklahoma

October 1985

Distribution:

1-2. J. Hamilton
3. E. M. Stefanski
4. R. W. Weeks
5. F. Y. Fradin
6. W. J. Shack
7. T. F. Kassner
8. P. S. Maiya
9. J. Y. Park
10. W. E. Ruther

To be presented at the 13th Water Reactor Safety Research Information Meeting, October 23-25, 1985, sponsored by the U.S. Nuclear Regulatory Commission, Washington, D. C.

*Work supported by the U.S. Nuclear Regulatory Commission. RSR FIN Budget No. A2212; RSR Contact: A. Taboada.

BWR Pipe Crack and Weld Clad Overlay Studies*

by

W. J. Shack, T. F. Kassner, P. S. Maiya,
J. Y. Park and W. E. Ruther

Materials Science and Technology Division
ARGONNE NATIONAL LABORATORY
Argonne, Illinois

and

E. F. Rybicki

E. F. Rybicki, Inc.
Tulsa, Oklahoma

October 1985

To be presented at the 13th Water Reactor Safety Research Information Meeting, October 23-25, 1985, sponsored by the U.S. Nuclear Regulatory Commission, Washington, D. C.

*Work supported by the U.S. Nuclear Regulatory Commission. RSR FIN Budget No. A2212; RSR Contact: A. Taboada.

BWR Pipe Crack and Weld Clad Overlay Studies*

by

W. J. Shack, T. F. Kassner, P. S. Maiya,
J. Y. Park and W. E. Ruther

Materials Science and Technology Division
ARGONNE NATIONAL LABORATORY
Argonne, Illinois

and

E. F. Rybicki

E. F. Rybicki, Inc.
Tulsa, Oklahoma

ABSTRACT

This paper presents results on (a) the influence of simulated BWR environments and temperature on the intergranular-stress-corrosion cracking (IGSCC) susceptibility of sensitized stainless steels (SS), (b) the stress-corrosion susceptibility of alternative piping materials, (c) analyses of field components to assess the effectiveness of in-service inspection techniques and the in-reactor performance of weld overlay repairs, and (d) finite-element analyses and experimental measurement of residual stresses in weldments with weld overlays. Fracture-mechanics crack-growth data are presented to confirm correlations between the critical corrosion potentials required to inhibit IGSCC and the level of impurities in the environment. Slow-strain-rate tests show that very low levels of impurities (25 ppb of sulfate) can produce susceptibility to transgranular-stress-corrosion cracking (TGSCC) in Type 316NG SS and that nitrogen levels in SS above 0.1 wt.% appear to increase susceptibility to TGSCC. Preliminary results on a German Type 347NG SS suggest that it is at least as resistant to TGSCC in impurity environments as Type 316NG SS. Measurements on overlay weldments removed from the Hatch-2 reactor confirm that compressive residual stresses are produced on the inner surface of the weldments by the overlay. Comparisons with full elastic-plastic finite-element solutions show that the elastic superposition solutions commonly used to analyze crack growth in overlay weldments may be unconservative, although for typical applied loads even the elastic-plastic solutions indicate that stress intensity factors at crack tips are negative for weldments with an overlay repair.

---

*Work supported by the U.S. Nuclear Regulatory Commission. RSR FIN Budget No. A2212; RSR Contact: A. Taboada.

INTRODUCTION

Leaks and cracks in the heat-affected zones of weldments in austenitic stainless steel (SS) piping in boiling water reactors (BWRs) due to intergranular-stress-corrosion cracking (IGSCC) have been observed since the mid-1960s. Since that time, cracking has continued to occur, and indications have been found in all parts of the recirculation system.

Proposed solutions for the problem include procedures that produce a more favorable residual stress state on the inner surface of weldments, materials that are more resistant to stress-corrosion cracking (SCC), and changes in the reactor environment that decrease the susceptibility to cracking. The objective of this program is an independent evaluation of these remedies and a better understanding of the weld-overlay procedure, which is the most widely used short-term repair for flawed piping.

TECHNICAL PROGRESS

Major efforts during the past year include (1) studies of the influence of environment and temperature on IGSCC susceptibility of sensitized stainless steels, (2) studies of the SCC susceptibility of alternative piping materials, (3) analyses of field components to assess the effectiveness of in-service inspection techniques and the in-reactor performance of weld overlay repairs, and (4) finite-element analyses and experimental measurement of residual stresses in weldments with weld overlays.

Influence of Environment and Temperature on IGSCC Susceptibility of Sensitized Stainless Steels

Both laboratory and in-reactor tests have shown that hydrogen additions to the reactor feedwater can reduce the susceptibility to IGSCC in the recirculation piping. The hydrogen can recombine with the dissolved oxygen in the reactor coolant in the presence of the strong radiation fields and thus lower the corrosion potential of the system. The level to which the potential must be decreased to inhibit cracking is strongly dependent on the type and level of impurities in the coolant. Our previous work [1] has established a correlation between this critical potential and the concentration of sulfuric acid based on constant extension rate (CERT) test results. This correlation can be expressed in terms of conductivity to be consistent with the more usual characterization of coolant chemistry in an operating plant, and is shown in the insert panel of Fig. 1. Since sulfate is a particularly deleterious impurity [2], it probably represents a conservative estimate of the potential that must be achieved to avoid IGSCC in a reactor environment.

Although CERT tests are very useful for the study of the effects of impurities, the large plastic strains produced in these tests are unrealistic, and fracture-mechanics crack growth rate tests have been performed to verify this potential-conductivity correlation under more prototypical loading conditions. Three 1TCT specimens of Type 304 SS (Heat No. 30956) in the solution-annealed and sensitized conditions (EPR = 0, 2, and 20 C/cm^2) were loaded in series, fatigue precracked at 289°C in air at a stress intensity

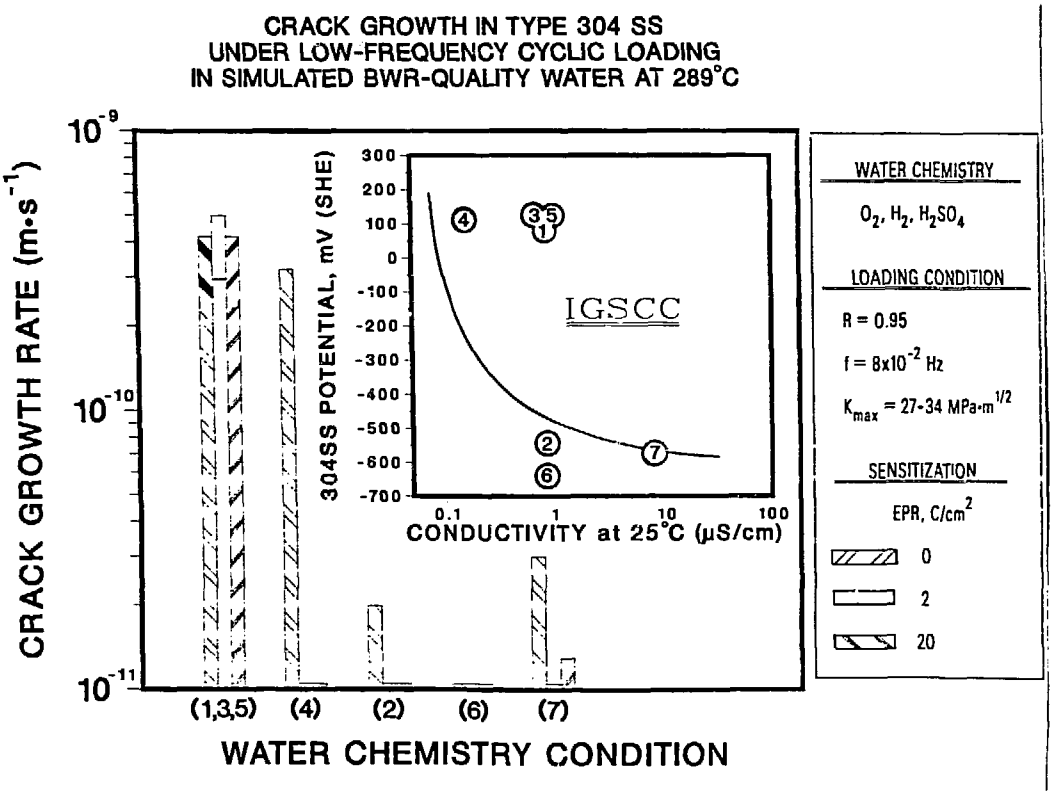

Fig. 1. Effect of Several Simulated BWR Water Chemistries within and Outside of the IGSCC Regime on the Crack Growth Rates of Compact-Tension Specimens of Type 304 SS with Different Levels of Sensitization under Low-Frequency, Moderate Stress-Intensity, and High-R Loading Conditions at 289°C.

Table I. Crack Growth Results for Type 304 SS Specimens[a] During an Experiment[b] in Which the Dissolved Oxygen and Sulfate Concentrations of the Feedwater were Cycled between a Reference Condition and Several Different Chemistries Including Hydrogen Additions to the Water

Test Cond.	Test Time, h	Water Chemistry: Oxygen,[c] ppm	Hydrogen, ppm	Sulfate, ppm	Cond., μS/cm	Electrode Potentials: 304 SS, mV(SHE)	Pt, mV(SHE)	Specimen #27 (EPR = 0 C/cm^2): Crack Length, mm	K_{max}, MPa·m$^{1/2}$	Growth Rate, m·s^{-1}	Specimen #28 (EPR = 2 C/cm^2): Crack Length, mm	K_{max}, MPa·m$^{1/2}$	Growth Rate, m·s^{-1}	Specimen #29 (EPR = 20 C/cm^2): Crack Length, mm	K_{max}, MPa·m$^{1/2}$	Growth Rate, m·s^{-1}
1	5	0.2-0.3	-	0.1	0.88	+80	+180	0.84	26.5		1.17	27.0		1.24	27.1	
	840							1.65		2.8×10^{-10}	2.67		5.0×10^{-10}	2.51		4.2×10^{-10}
2	1007	0.002	-	0.1	0.88	-545	-520	1.73	27.8		2.67	29.1		2.51	28.9	
	2184							1.80		2.0×10^{-11}	2.62		0	2.49		0
3	2357	0.2-0.3	-	0.1	0.88	+120	+215	2.01	28.1		3.25	30.0		2.79	29.3	
	3024							3.04		4.2×10^{-10}	4.06		3.4×10^{-10}	3.61		3.4×10^{-10}
4	3196	0.2-0.3	-	-	0.16	+110	+230	3.25	30.0		4.06	31.5		3.58	30.5	
	4200							4.39		3.2×10^{-10}	4.09		0	3.58		0
5	4393	0.2-0.3	-	0.1	0.88	+120	+190	4.72	32.3		4.78	32.4		4.11	31.4	
	5040							5.69		4.2×10^{-10}	5.46		2.9×10^{-10}	4.72		2.6×10^{-10}
6	5208	0.002	1.4	0.1	0.88	-635	-640	5.74	34.0		5.46	33.7		4.70	32.3	
	6216							5.77		0	5.41		0	4.62		0
7	6385	0.002	1.4	1.0	8.1	-575	-565	5.79	34.1		5.41	33.4		4.64	32.2	
	7011							5.82		3.0×10^{-11}	5.25		0	4.67		1.3×10^{-11}

[a]Compact tension specimens (1TCT) from Heat No. 30956 were solution annealed at 1050°C for 0.5 h (EPR = 0), sensitized at 700°C for 12 h (EPR = 20 C/cm^2), and 700°C for 0.25 h plus 500°C for 24 h (EPR = 2 C/cm^2).

[b]The load ratio and frequency of the positive sawtooth waveform were 0.95 and 8×10^{-2} Hz, respectively.

[c]Feedwater oxygen concentration at the 0.2-0.3 ppm level was approximately a factor of 3 higher to compensate for oxygen depletion by corrosion of the autoclave system.

K_{max} of ∿20 MPa·$m^{\frac{1}{2}}$ and a frequency of 10 Hz, and then tested at a load ratio (R) value of 0.95 and K_{max} = 28 MPa·$m^{\frac{1}{2}}$, under a positive sawtooth waveform at a frequency of 8 x 10^{-2} Hz.

The water chemistry conditions were varied from a reference condition of 0.2 ppm dissolved oxygen with 0.1 ppm sulfate (as H_2SO_4) to lower oxygen concentrations at this sulfate level as well as higher and lower sulfate concentrations at a fixed dissolved oxygen concentration in the feedwater. The temperature was maintained at 289°C for the entire test. Measurements of the steady-state open-circuit corrosion potential of the steel and the redox potential of a platinum electrode located at the outlet of the autoclave were made and analyses of the inlet and effluent dissolved oxygen concentrations of the water were obtained during each water chemistry condition. Steady-state crack growth rates were determined over time intervals of ∿600 to 1000 h. The times required to establish steady-state water chemistry conditions were short compared to the periods used to measure crack growth rates.

The crack growth data are shown in Fig. 1 and tabulated in Table I along with the electrochemical-potentials and the dissolved oxygen, hydrogen, and sulfate concentrations during each phase (numbered from 1-7) of the experiment. The open-circuit corrosion potential of the steel and the conductivity of the feedwater for each phase of the test along with the region of susceptibility to IGSCC based on CERT test data [1,2] are also shown in the insert panel of Fig. 1.

The crack growth rates under the reference water chemistry phases [(1,3, 5) in Fig. 1] ranged from 2.8-5.0 x 10^{-10} m s^{-1} for the three different levels of sensitization. In phase 2, in which the dissolved oxygen concentration of the water was decreased from 0.2 to 0.002 ppm, crack growth in the sensitized specimens ceased, and the rate in the solution-annealed specimen decreased by a factor of ten. When the reference water chemistry was restored, i.e., phase 3, the crack growth rates resumed at the initial rates. During phase 4, the dissolved oxygen concentration was maintained at 0.2-0.3 ppm, but sulfate was not added to the feedwater. Crack growth in the sensitized specimens again ceased, but crack growth in the solution-annealed specimen continued at approximately the same rate as before. Although the conditions during phase 4 still fall within the region of susceptibility to IGSCC, the lower crack growth rates reflect the benefit of improved water chemistry (i.e., lower impurity levels) even at the 0.2-0.3 ppm dissolved oxygen level.

After crack growth under the reference water chemistry condition was resumed, i.e., phase 5, the oxygen concentration of the effluent was decreased to 0.002 ppm, and 1.4 ppm hydrogen was added to the feedwater (phase 6). During this change the steady-state open-circuit corrosion potential of the steel decreased from +120 to -635 mV (SHE), and crack growth ceased in all of the specimens in agreement with predictions based on the CERT test data. In the last phase of the experiment, the sulfate concentration of the feedwater, containing 0.002 ppm dissolved oxygen and 1.4 ppm hydrogen, was increased from 0.1 to 1.0 ppm. This condition falls on the boundary of a region of IGSCC susceptibility in Fig. 1, and during this phase the corrosion potential of the

steel increased slightly, primarily due to the decrease in pH of the water, and crack growth resumed in the solution-annealed and moderately sensitized specimens, but at a relatively low rate ($<3.0 \times 10^{-11}$ m s^{-1}).

The fracture surface morphology and crack path in the solution-annealed specimen (EPR = 0) were transgranular, whereas for the lightly (EPR = 2 C/cm^2) and moderately (EPR = 20 C/cm^2) sensitized specimens intergranular cracking occurred. Under almost all water chemistry conditions, the highest crack growth rates were observed in the solution-annealed material. Thus the superior in-reactor performance of solution-annealed materials appears to rest on their resistance to crack initiation and not an inherent resistance to crack propagation.

In general, the crack growth results from the fracture-mechanics-type specimens are consistent with the predictions of susceptibility to IGSCC based on CERT test data. However, to a certain extent the fracture-mechanics tests indicate greater susceptibility to environmentally enhanced cracking, since only at extremely low potentials was crack growth completely halted for all heat treatment conditions.

A strong synergistic interaction between the effects of impurities (i.e., sulfate added as H_2SO_4) and temperature has been observed in CERT tests. Results for temperatures from 140 to 320°C and sulfate levels of 0, 0.1 and 1.0 ppm are shown in Fig. 2 [3]. In high purity water there is a large decrease in crack growth rates and a change in cracking mode from intergranular to transgranular and ultimately to ductile as the temperature was increased to 320°C. In the presence of impurities, however, intergranular cracking and high crack growth rates occur even at the highest temperatures. Fracture-mechanics crack growth tests were performed to confirm these results. Steady-state crack growth was established in three specimens with sensitization levels of 0, 2, and 20 C/cm^2 over a period of ∿1400 h in high-purity water (0.15 μS/cm) with 0.2-0.3 ppm dissolved oxygen at 289°C (Fig. 3). At the end of this period, the temperature was raised from 289 to 320°C with the same feedwater chemistry, and the pressure was increased from 8.6 to 12.5 MPa to prevent boiling. Crack growth in the two sensitized specimens virtually ceased over the subsequent 1400-h period at 320°C as predicted by the CERT test results. In the last phase of the experiment, the temperature was decreased to 289°C under the same total pressure, water chemistry, and load conditions. Crack growth in the sensitized specimens resumed at approximately the same rates as in the first phase of the experiment.

The transition in fracture mode from intergranular to transgranular (and ultimately to 100% ductile failure) in the CERT tests, and the sharp decrease in the crack growth rates in both the CERT and fracture-mechanics tests with increasing temperature, are consistent with the variation of the corrosion potential of the steel with temperature. As shown in Fig. 4, the steady-state corrosion potential of the steel decreases rapidly above ∿250°C. If the dependence of the fracture mode on corrosion potential and water purity at 320°C is similar to that at 289°C (see inset panel in Fig. 1), a relatively small decrease in potential [i.e., from +100 to ∿0 mV (SHE)] as the temperature

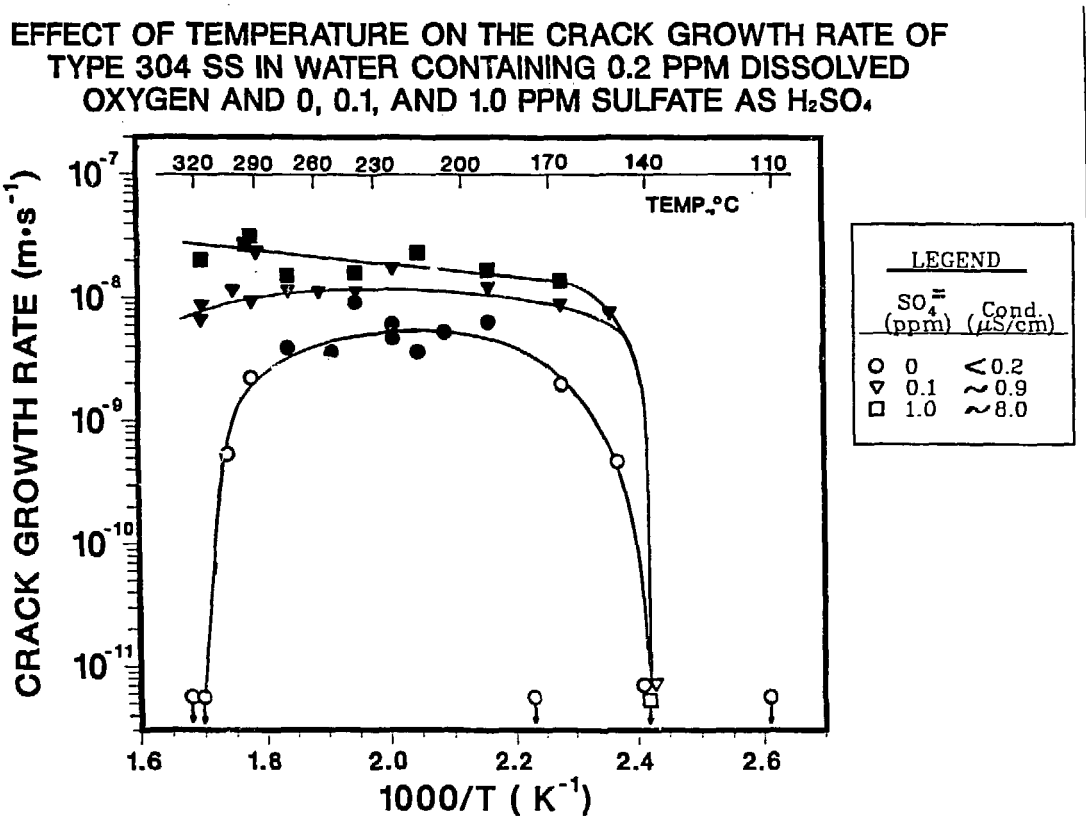

Fig. 2. Effect of Temperature on the Crack Growth Rate of Sensitized (EPR = 2 C/cm^2) Type 304 SS Specimens from CERT Tests at a Strain Rate of 1 x 10^{-6} s^{-1} in Water Containing 0.2 ppm Dissolved Oxygen and 0, 0.1, and 1.0 ppm Sulfate as H_2SO_4. Open and closed symbols denote either ductile or ductile plus transgranular and ductile plus intergranular fracture morphology, respectively.

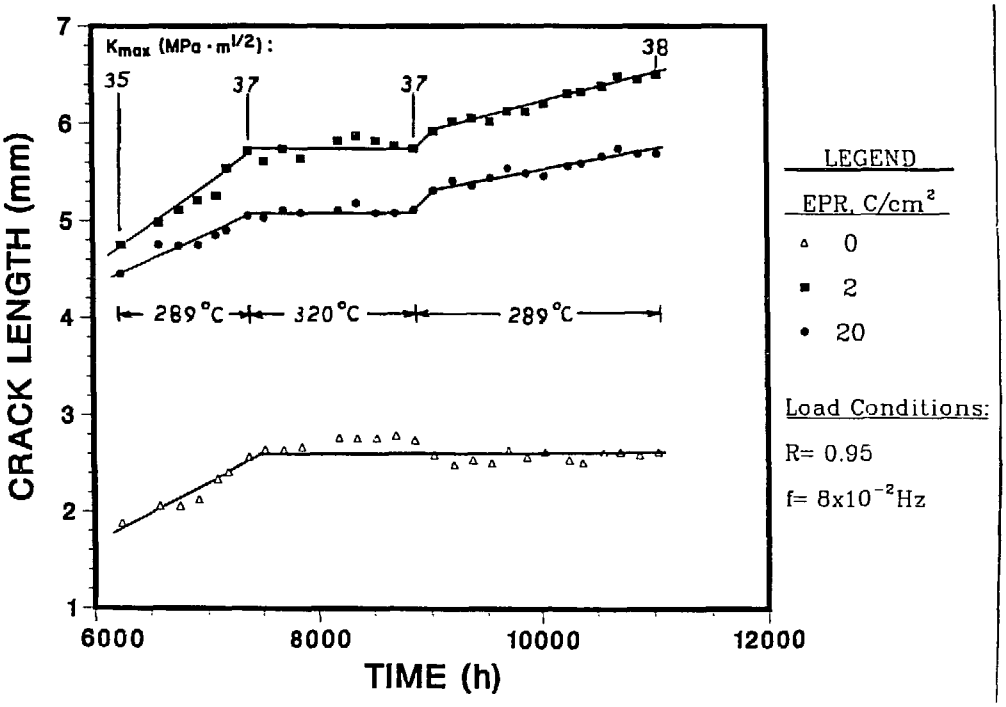

Fig. 3. Crack Length versus Time for 1TCT Specimens of Solution-annealed (EPR = 0) and Sensitized (EPR = 2 and 20 C/cm^2) Type 304 SS in High-Purity Water Containing 0.2 ppm Dissolved Oxygen at 289 and 320°C.

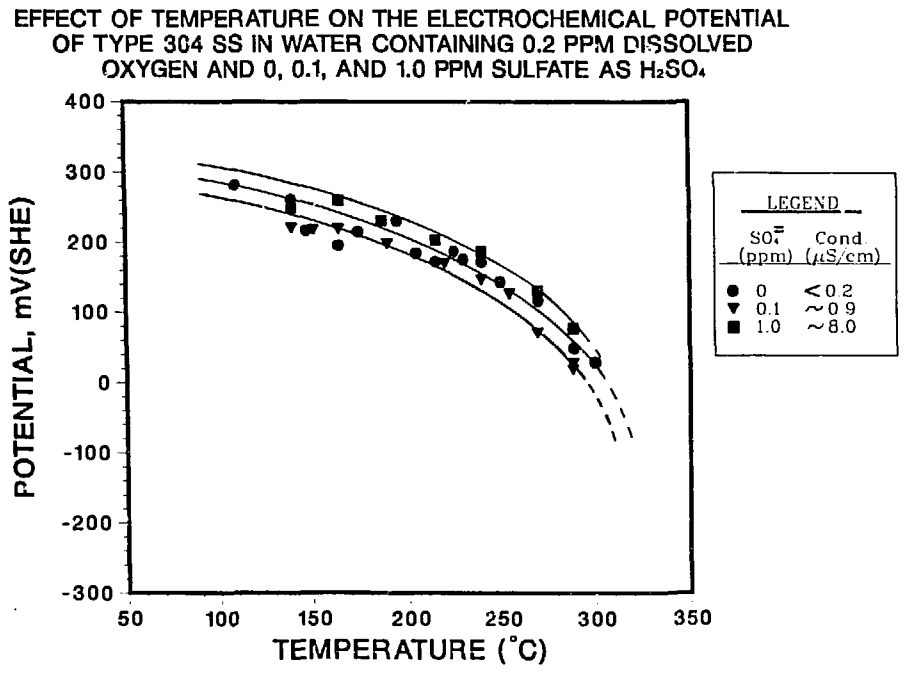

Fig. 4. Effect of Temperature on the Electrochemical Potential of Type 304 SS in Water Containing 0.2 ppm Dissolved Oxygen 0, 0.1, and 1.0 ppm Sulfate as H_2SO_4.

increases could account for the change in fracture mode and the concomitant decrease in the crack growth rate of the steel in high-purity water.

SCC Susceptibility of Type 316NG SS

Our previous work [4-5] has shown that Type 316NG SS in susceptible to transgranular-stress-corrosion cracking (TGSCC) in oxygenated water (0.2 ppm O_2) with impurities (0.1 ppm sulfate, added as acid). Although this impurity level is within the Reg. Guide 1.56 limits, it is much higher than is typical for operating plants. CERT test results for lower impurity concentrations and two strain rates, 4×10^{-7} and 2×10^{-7} s^{-1}, are summarized in Table II. Although no cracking occurs in high purity water, TGSCC occurs in low conductivity water (0.25 µS/cm) containing sulfate levels as low as 0.025 ppm. The test results indicate that at a strain rate of 2×10^{-7} s^{-1}, the critical sulfate concentration needed to induce cracking is between 0.01 and 0.025 ppm. This level could even be lower at slower strain rates. Despite some scatter in the data, it also appears that, although cracking occurs even at low impurity levels, the crack growth rates decrease with decreasing impurity concentration.

TGSCC of solution-annealed Type 304 SS has also been observed in CERT tests in impurity environments. TGSCC does not appear to be a significant problem in existing Type 304 SS piping systems. However, it is possible that, at present, cracking incidents are dominated by the more severe IGSCC in sensitized stainless steels, and TGSCC could occur in nuclear grade systems, albeit at a lower frequency, unless other measures are taken, such as good water chemistry control or residual stress remedies.

To assure that TGSCC in impurity environments is not an artifact associated with the large plastic strains achieved in CERT tests, interrupted tests were performed on Types 316NG and 316 SS in oxygenated water (0.02-0.2 ppm) containing 0.1 ppm sulfate at strain rates between 10^{-6} and 10^{-7} s^{-1}. In these tests cracks 50-200 µm long are observed at relatively small strains (<5%). The results are consistent with predictions of our phenomenological model for crack growth in CERT tests and the assumption that initiation of smaller cracks (∿1 µm deep) occurs at much lower strains (∿1%), but direct observation at lower strains is difficult.

Fracture-mechanics crack growth rate tests are also being performed to confirm the predictions of the CERT tests. Companion 1TCT specimens of sensitized Type 304 SS (EPR = 2 C/cm^2) and Type 316NG SS are being tested at 289°C in an environment containing 0.2 ppm dissolved oxygen and 0.1 ppm sulfate at a stress intensity value K of ∿29 MPa $m^{\frac{1}{2}}$ and a load ratio R = 0.95 under a sawtooth waveform with a frequency of 8×10^{-2} Hz. The crack growth rates for Types 304 and 316NG SS specimens are 2.8×10^{-10} m/s and 1.6×10^{-10} m/s, respectively, which is consistent with the relative crack growth rates observed in CERT tests under these conditions.

Table II. CERT Test Results for Type 316NG SS[a] in 289°C Oxygenated Water (~0.2 ppm) with Several Sulfate Concentrations

Test No.	Sulfate, ppm	Conductivity, μS/cm	t_f, h	σ_{max}, MPa	Failure Mode	$\dot{a}_{av}$, m/s
			$\dot{\varepsilon} = 4 \times 10^{-7}\ s^{-1}$			
169	0.1	0.90	217.4	462	TGSCC	9.74×10^{-10}
216	0.075	0.69	559.4	449	TGSCC	2.03×10^{-10}
			$\dot{\varepsilon} = 2 \times 10^{-7}\ s^{-1}$			
187	0.00	<0.2	483.3	460	Ductile	-
207	0.01	<0.2	497.3	468	Ductile	-
228	0.025	0.25	473.8	462	TGSCC	4.71×10^{-10}
210	0.025	0.25	532.4	458	TGSCC	6.33×10^{-10}
199	0.050	0.47	588.7	449	TGSCC	2.21×10^{-10}
228	0.075	0.64	562.8	456	TGSCC	4.52×10^{-10}
172	0.10	0.90	474.0	461	TGSCC	7.35×10^{-10}

[a]Heat No. P91576 after a heat treatment of 1050°C/0.5 h plus 650°C for 24 h.

Effect of Nitrogen Additions on SCC Susceptibility

Although low carbon stainless steels are much more resistant to sensitization than conventional grades, the lower carbon levels generally lead to some loss in mechanical properties. The addition of nitrogen can restore much of this loss. In Types 304 and 316NG SS produced in the U.S., the nitrogen level is required to be between 0.06 and 0.10 wt.%. In Japan the nuclear grade steels may have up to 0.12 wt.% nitrogen, and LN materials may have up to 0.14 wt.% nitrogen. The basic deformation mechanisms associated with higher nitrogen levels can cause increased susceptibility to SCC. For example, an increase in nitrogen content may accelerate the oxide-film rupture process by promoting slip planarity. To investigate the possible detrimental effects on nitrogen additions CERT tests were performed on four heats of Types 316LN SS. The data from these tests as well as data on NG and conventional steels are plotted in Fig. 5 to show the variation of the TGSCC crack growth rate with nitrogen content. Nitrogen levels in excess of 0.1 wt.% appear to have an adverse effect on TGSCC.

SCC Susceptibility of Type 347 Stainless Steel

In a cooperative effort with the EPRI NDE Center, studies are being carried out on the German Type 347NG SS (Mannesmann TP347 DIN 1.4550). The work at the NDE Center focuses on weldability, and the work at ANL focuses on the SCC susceptibility of the material. Metallographic examination and CERT tests have been performed at ANL on weldments prepared at the NDE Center by the German GTAW process. An ASTM A262-A test showed no significant grain boundary precipitation except very near the weld fusion line. Shallow cracking (about 75 μm deep) was observed at the weld fusion line of the inner surface of pipe, and a weld defect (cavity) was also observed at the fusion line (Figs. 6 and 7).

CERTs have been performed in 289°C water with 0.2 ppm O_2 and 0.1 ppm sulfate on one heat of material (Heat No. 174100) in the as-welded condition and after an additional heat treatment (i.e., as-welded +500°C/24 h). The results are shown in Table III. Although a detailed examination of fracture surfaces has not yet been made, it is clear that TGSCC does occur in impurity environments. However, it has been observed only at strain rates of $\leq 5 \times 10^{-7}$ s^{-1}, which are slower than those required to produce TGSCC in CERT tests on Type 316NG SS. Hence, based on the data obtained to date, Type 347 SS, although not immune to transgranular cracking, appears slightly superior to Type 316NG SS.

Preliminary examination suggests that the cracks do not occur in the region immediately adjacent to the weld fusion line (the "knife-line attack" region). There does appear to be a consistent decrease in failure strain, though small, as a result of second heat treatment, which is intended to simulate aging in service.

Effects of Impurity Elements in Type 304 SS on SCC Susceptibility

The effect of impurity elements such as sulfur and phosphorus in austenitic stainless steels on SCC has been a subject of study and conjecture, but concrete

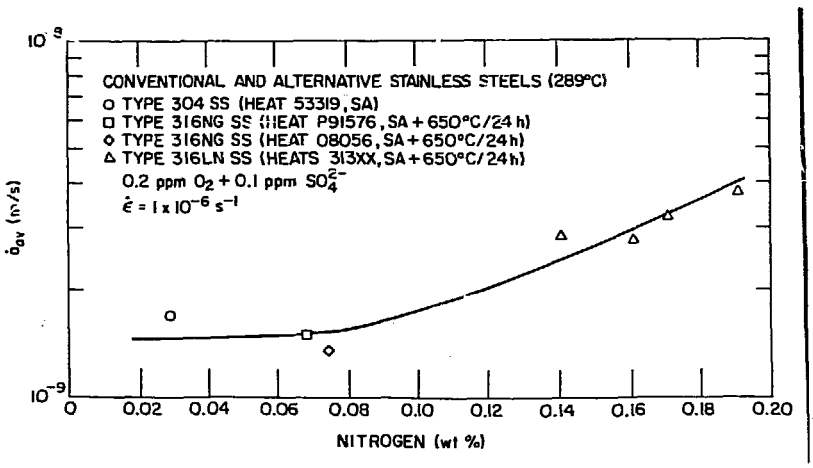

Fig. 5. Influence of Nitrogen on Average Transgranular Crack Growth Rates for Austenitic Stainless Steels.

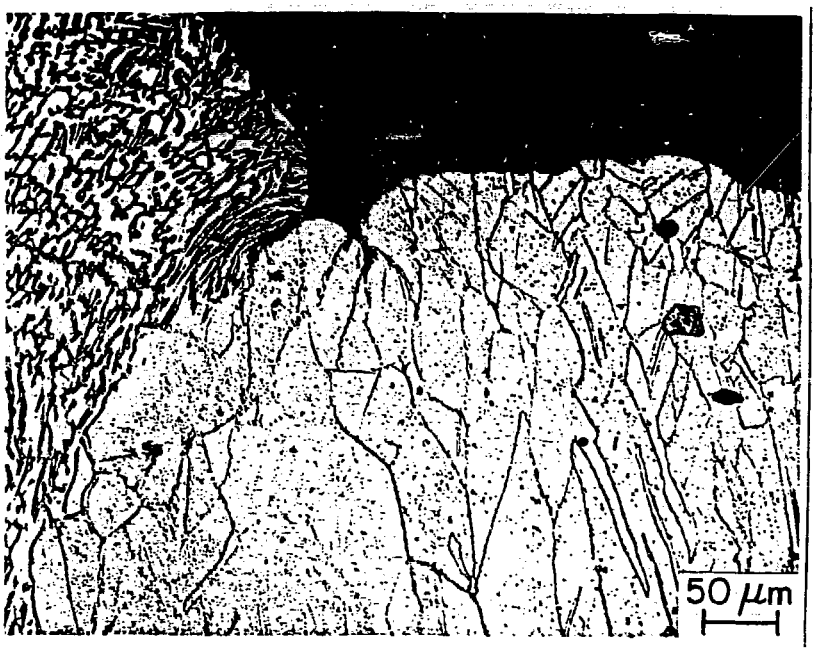

(a)

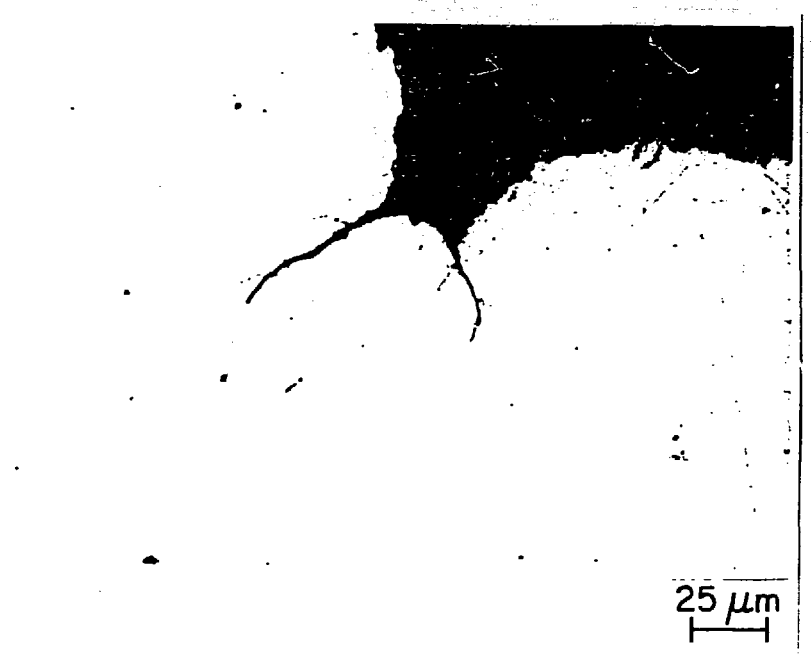

(b)

Fig. 6. (a) Cracks near Weld Fusion Line at Inner Surface of Type 347 SS Pipe Weldment. Electrolytically etched with 10% oxalic acid. (b) Cracks near weld Fusion Line at Inner Surface of Type 347 SS Pipe Weldment.

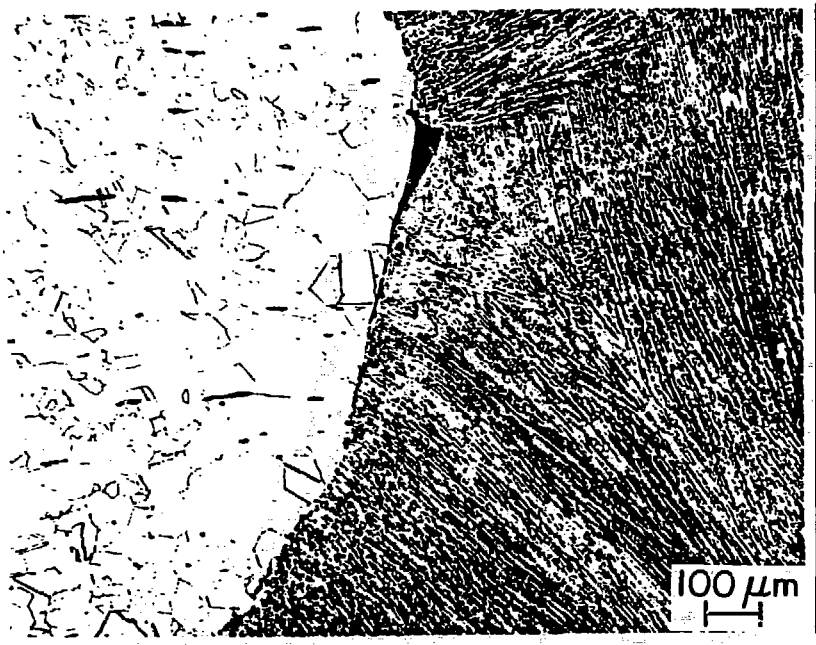

(a)

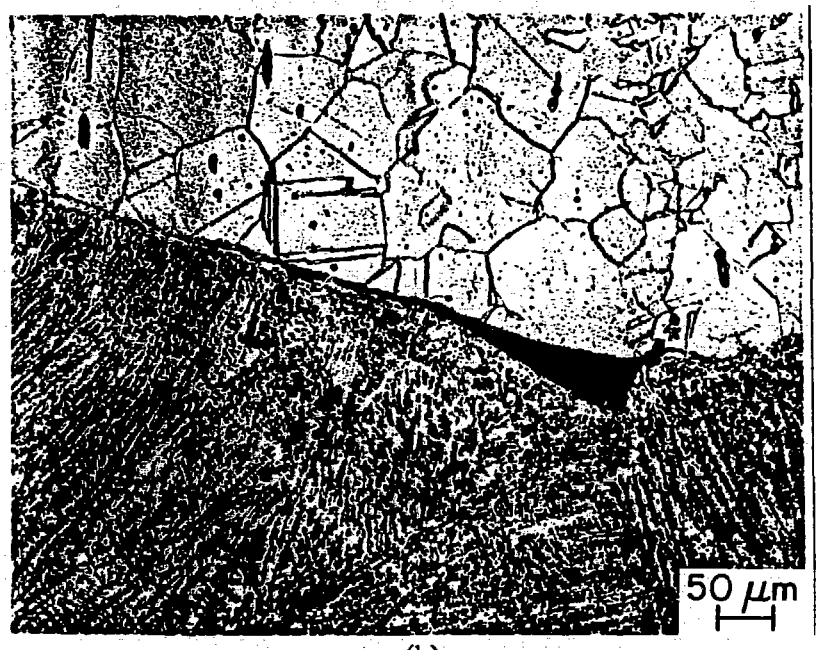

(b)

Fig. 7. (a) Cavity at Weld Fusion Line of Type 347 SS Pipe Weldment. (b) Cavity at Weld Fusion Line of Type 347 SS Pipe Weldment. Enlarged view of above photo.

Table III. CERT Test Results for Type 347 Stainless Steel in 289°C Water Containing ∿0.23 ppm Oxygen and 0.1 ppm Sulfate[a]

Specimen No.	Heat Treatment	t_f, h	ε_f, %	$\varepsilon_{uniform}$, %	σ_{max}	$\dot{\varepsilon}$, s^{-1}	Failure Mode
174-1	AW	77.5	27.9	19.4	435	1×10^{-6}	Ductile
174-4	AW + 500°C/24 h	65.5	23.6	18.2	432	1×10^{-6}	Ductile
174-2	AW	136.6	24.6	19.0	428	5×10^{-7}	TGSCC
174-5	AW + 500°C/24 h	114.5	20.6	16.6	417	5×10^{-7}	↓
174-8	AW	328.5	23.7	19.9	434	2×10^{-7}	
174-3	AW + 500°C/24 h	301.5	21.7	17.8	448	2×10^{-7}	
174-9	AW	676.5	24.4	21.6	443	1×10^{-7}	
174-6	AW + 500°C/24 h	574.5	20.7	16.4	451	1×10^{-7}	

[a]Steady-state open-circuit corrosion potential: ∿30 mV (SHE).

evidence of their role is difficult to obtain. Although low carbon stainless steels are less likely to undergo IGSCC due to the familiar process of chromium depletion by carbide precipitation at grain boundaries, the segregation of impurity elements to grain boundaries offers another possible mechanism for IGSCC.

Preliminary studies on conventional Type 304 SS show that impurity elements can also influence the grain boundary depletion of chromium. Scanning-electron-transmission microscopy (STEM) showed that phosphorus strongly promotes chromium depletion at low temperatures whereas sulfur does not (Fig. 8-9). ASTM A262-A test results were consistent with the STEM observations. After aging for 300 h at 550°C, the specimens doped with 0.09% P showed grain boundary ditching, while the specimens doped with 0.02% P or with sulfur did not. Future tests are planned on low carbon stainless steels doped with sulfur or phosphorus to determine the effect of these impurities on susceptibility to IGSCC when grain boundary carbide precipitation is negligible.

Analysis of Field Components with Weld Overlays

Laboratory ultrasonic examination, dye penetrant examination, residual stress measurements, metallographic examination, and sensitization measurements were performed on two 22-in. dia Type 304 SS pipe-to-endcap weldments (nos. 2B31-1RC-22BM-1 and xxx-1RC-22AM-x) with wled overlays that were removed from the primary coolant recirculation header piping of the Hatch-2 reactor operated by the Georgia Power Company.

These weldments were repaired when in-service-inspection revealed 360° intermittent crack indications. After repair the reactor was returned to service for approximately 18 months. The piping system was then replaced and the weldments sent to Argonne for analysis.

The width and the thickness of the overlay are ∿200 mm and 10-15 mm for the weldment 22 BM, and 230 mm and 9-10 mm for weldment 22 AM. Although the inner surface of the pipe was electropolished by Quadrex Inc. to remove the corrosion film and reduce radiation levels, postweld grinding marks were visible at the inner surface of the weld crown and the heat-affected zone (HAZ).

Ultrasonic examinations showed that it is very difficult to differentiate crack signals from root signals when inspecting weldments with overlays because of the low signal-to-noise ratio. A more detailed discussion of the results of the ultrasonic examination is given in another paper at this conference [6].

Dye penetrant examinations revealed a number of axial, circumferential, and skewed indications in a localized area (10% of the total circumference) on the endcap side of one of the weldments (no. 2B31-1RC-22BM-1). The indications were located within 10 mm of the weld fusion line, and postweld grinding had been performed on this region. No dye penetrant indications were observed in the other weldment.

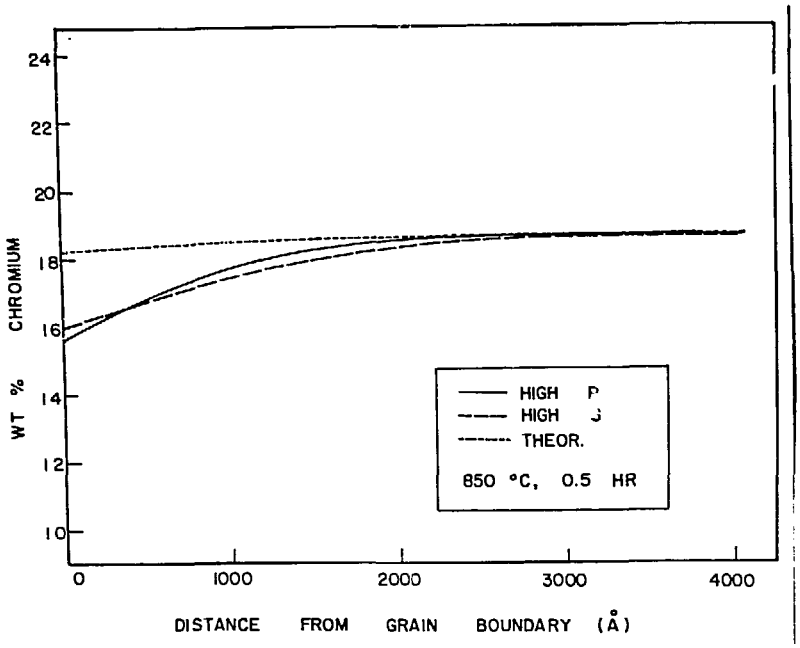

Fig. 8. Measured Chromium Concentration near Grain Boundary of Type 304 SS Doped with 0.09% P or S Concentration and Aged at 850°C for 0.5 h, and Calculated.

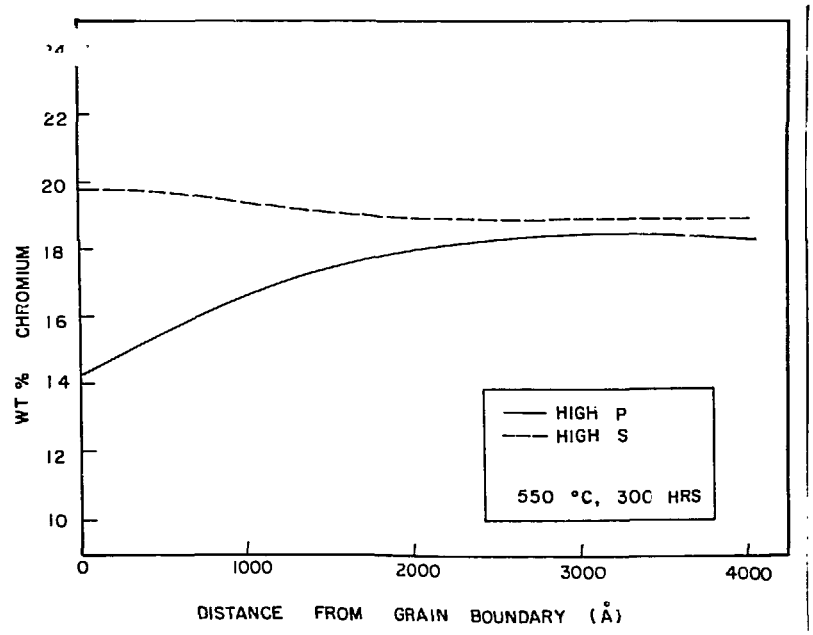

Fig. 9. Measured Chromium Concentration near Grain Boundary of Type 304 SS Doped with 0.09% P or S, and Aged at 550°C for 300 h.

After ultrasonic and dye penetrant examination, the weldments were sectioned. Cross-sections were metallographically polished and examined for cracks, defects, or any other features that might have caused the ultrasonic and dye penetrant indications. The dye penetrant indications were associated with axial and circumferential intergranular cracks that were up to 14.6 mm deep (35% of the total wall thickness including the overlay). There were no discernible structural features observed in the cross sections where ultrasonic indications were noted but no dye penetrant indications were observed. ASTM A262-A tests showed the region of cracking was sensitized and that the HAZ on the outer surface produced by the overlay welding did not extend more than 7 mm throughwall from the fusion line. The ferrite content of the original weld was 6% and 15% for the overlay.

In general, our observations and conclusions are similar to those from the previous analyses of two pipe-elbow overlay weldments from Hatch-2. Relatively few, short cracks were present, although several of the cracks were quite deep (35-60% throughwall). There was no evidence of tearing or throughwall extension of the cracks due to overlay welding. In the two weldments in which cracking occurred, the forged component (elbow or endcap) showed more extensive cracking than the pipe.

Residual stresses were also measured on a pipe-to-endcap overlay weldment (2B31-1RC-22BM-1) and a 12-in. pipe-to-elbow overlay weldment (2B31-1RC-12RC-0-3). After the weldments were instrumented with strain gages, full-thickness specimens were cut from the weldment. To determine the stresses on the inner surface, thin sections (3 mm) were removed from the inner surface of each specimen by electrical discharge machining to provide almost complete stress relief for the gages on the inner surface.

The results for the pipe-to-elbow weldment are shown in Table IV. The 0° position is at the extrados of the elbow; the 180° position is at the intrados of the elbow. The 90° and 270° positions are on the midplane of the elbow. A number of rosettes were lost during the machining operations so that measurements were not obtained at all intended positions. The measured stresses on this weldment are much less axisymmetric than those measured on companion mock-up weldments; as might be expected, the asymmetry seems stronger on the elbow side. The stresses on the inner surface are compressive, although not as compressive as those obtained on the mock-up weldments. This could be attributed to the increased flexibility due to the elbow, which could accommodate the shrinkage due to the overlay, but other explanations are also possible.

The residual stresses measured on the inner surface of the pipe-to-endcap weldment are summarized in Table V. In the table, the gage locations are described in terms of distance around the circumference (40 cm, 60 cm, etc.) and a letter p or c denoting whether the rosette is located on the pipe or the cap side, respectively. The stresses are similar in character to those measured on mock-up weldments and those calculated by finite-element techniques. Both the axial and hoop stresses are strongly compressive. The distribution appears relatively uniform around the circumference, unlike the elbow-pipe weld.

Table IV. Measured Residual Stresses on a Hatch 12-in. Elbow-to-Pipe Overlay Weldment

	Azimuth				
	0	90	180	270	
Inner Surface					
Pipe Side	-15	-10	-21	-15	Axial Stress (ksi)
	-105	-70	-147	-105	(MPa)
	-37	-27	-66	-45	Hoop Stress (ksi)
	-259	-189	-462	-315	(MPa)
Elbow Side	-31	-11	-60		Axial Stress (ksi)
	-217	-77	-420		(MPa)
	-42	-29	-55		Hoop Stress (ksi)
	-294	-203	-385		(MPa)
Outer Surface					
Pipe Side	25	32			Axial Stress (ksi)
	175	224			(MPa)
	5	10			Hoop Stress (ksi)
	35	70			(MPa)
Elbow Side	0				Axial Stress (ksi)
	0				(MPa)
	-15				Hoop Stress (ksi)
	-105				(MPa)

Finite-Element Studies of Stresses Associated with Overlays

Most fracture-mechanics analyses of crack growth that may occur after application of weld overlays to weldments with cracks have been based on elastic superposition arguments. The stress intensity at the crack tip due to the residual stresses is then assumed equal to that due to applied stresses, equal in magnitude to the residual stresses for the uncracked weldment but opposite in sign, acting on the crack faces. Although such a superposition argument is valid for elastic loading, the application of a weld overlay and the development of residual stresses are inherently elastic-plastic processes.

Table V Measured Residual Stresses on a 22-in. Pipe-to-Endcap Overlay Weldment

Gage Position	Inner Surface Residual Stresses	
	Axial Stress (ksi)	Hoop Stress (ksi)
40 cm-p*	-30	-50
60 cm-c*	-22	-43
80 cm-p	-23	-59
95 cm-c	-20	-43
120 cm-c*	-22	-46
175 cm-c*	-24	-82

*Because of difficulties encountered in laying gages on radioactive piping, a gage in the rosette at this location was inoperative. The stresses were calculated assuming that the axial and hoop directions were principal stress directions. Comparisons with locations where complete rosettes were available and with measurements on other overlays indicate that the error in the axial stress introduced by this approximation is <15%.

To gain insight into the accuracy of the elastic superposition approach, two complete elastic-plastic finite-element solutions were compared with the simpler elastic superposition solutions. In the full elastic-plastic solution, the effect of an overlay on a weldment with a preexisting crack is computed. During the computation, the crack opening is monitored so that the compressive stresses associated with crack closure are properly modeled. The redistribution of stress with plastic deformation is also considered. The calculation must be repeated for each crack length of interest with this approach, which is very expensive. In contrast, the elastic superposition method requires only a single elastic-plastic solution for the residual stress distribution in an uncracked weldment. The stress intensity for an arbitrary crack depth can then be obtained by an inexpensive elastic calculation.

The stress intensity factors for the elastic-plastic finite-element solutions were calculated by use of the well known relationship between the energy release rate and the stress intensity factor. For consistency, the same approach was also used to compute the stress intensity factors for the elastic superposition method. However, in most analyses based on superposition, the stress intensity factors are not calculated using energy release rates. Instead, an influence function approach is used to compute stress intensity factors by simple quadrature after the residual stresses for the uncracked weldment are determined [7]. For completeness, this method was also used to compute stress intensity factors.

Calculations were carried out for 12-in. weldments with complete circumferential cracks, 20% and 60% throughwall, respectively. A 4-in. long overlay was applied to the weldment with the 20% throughwall crack and a 3-in. long overlay was applied to the weldment with the 60% throughwall crack. The overlay thickness in both cases was ∿3 mm. Stress intensity factors for complete circumferential cracks from the full elastic-plastic solutions for crack depths of 20% and 60%, from the elastic superposition finite-element solutions, and from the influence function solutions are shown in Fig. 10. The discrepancy between the two elastic solutions may be due to the effect of the circumferential stresses, which are not considered in the influence function approach, or to the differences in residual stresses between the polynomial fit used for the influence function calculations and the actual finite-element results.

The elastic superposition approach (based either on the finite-element energy release-rate calculation or the influence function method) gives less conservative estimates of the stress intensity than complete elastic-plastic solutions. For example, the elastic-plastic solutions show that for the 60% throughwall crack the stress intensity is positive for an applied axial stress of 15 ksi, while the simpler elastic solutions predict large negative stress intensity factors. However, for typical applied loads the elastic-plastic calculations, even for the large cracks modeled in these examples, give negative stress intensity factors, and although the stress intensity factor is positive for the weldment with a deep crack under a high axial load, it is much less than the corresponding stress intensity factor for a cracked weldment without an overlay.

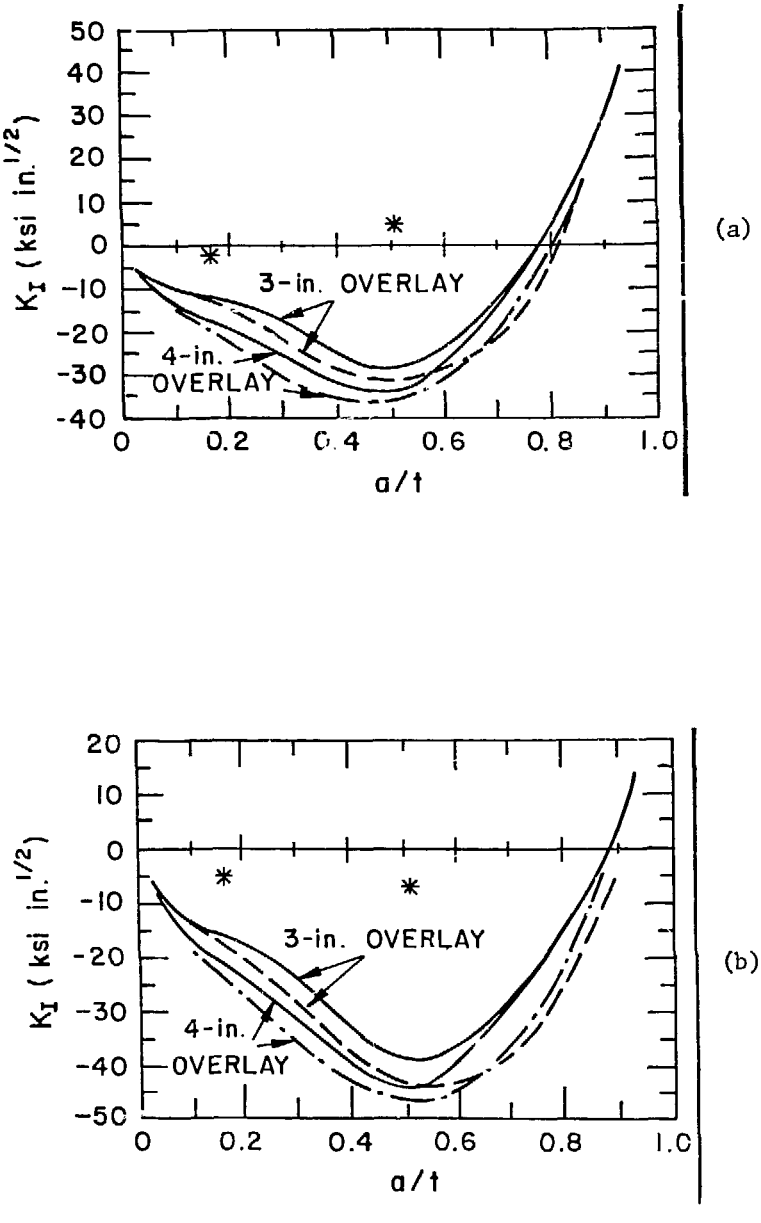

Fig. 10. Stress Intensity Factors Obtained by Elastic Superposition of Residual Stresses and Applied Stresses as a Function of Crack Depth. Stress intensity factors obtained by full elastic-plastic calculations for two crack depths are indicated by asterisks. Stress intensity factors obtained by influence function calculations are indicated by dashed curves. (a) 9 ksi applied axial stress; (b) 15 ksi applied axial stress.

FUTURE WORK

Studies will be performed to assess the possible effects of grain boundary segregation and cold work on stress-corrosion cracking of low carbon stainless steels in BWR environments. Residual stress distributions associated with the mechanical stress improvement process (MSIP) will be measured. The effects of intense gamma radiation on corrosion potentials and the effectiveness of low oxygen levels in inhibiting SCC in irradiated materials will be examined. The effects of impurities on crack growth rates in Type 308 weld metal will be studied. Low-stress cyclic-loading pipe tests on welded pipes are in progress to assess the effect of impurities under more prototypic loading conditions. Long-term aging studies on nuclear grade and conventional materials will continue.

REFERENCES

1. W. E. Ruther, W. K. Soppet, and T. F. Kassner, in Environmentally Assisted Cracking in Light Water Reactors: Annual Report, October 1982--September 1983, NUREG/CR-3806, ANL-84-36 (June 1984), pp. 101-117.

2. W. E. Ruther, W. K. Soppet, and T. F. Kassner, in Light-Water-Reactor Safety Materials Engineering Research Programs: Quarterly Progress Report for April-June 1984, NUREG/CR-3998 Vol. II, ANL-84-60 Vol. II (February 1985), pp. 38-47.

3. W. E. Ruther, W. K. Soppet, and T. F. Kassner, in Environmentally Assisted Cracking in Light Water Reactors: Annual Report, October 1983--September 1984, NUREG/CR-4287, ANL-85-33 (June 1985), pp. 93-113.

4. P. S. Maiya and W. J. Shack, in Light-Water-Reactor Safety Research Program: Quarterly Progress Report for October-December 1983, NUREG/CR-3689 Vol. I, ANL-83-85, Vol. IV, (August 1984), pp. 31-50.

5. P. S. Maiya and W. J. Shack, in Environmentally Assisted Cracking in Light Water Reactors: Annual Report, October 1983-September 1984, NUREG/CR-4287, ANL-85-33 (June 1985), pp. 27-61.

6. D. S. Kupperman, T. N. Claytor, D. W. Prine, and T. A. Mathieson, Leak Detection and Nondestructive Examination of Stainless Steel, these Proceedings.

7. D. D. Dedhia and D. O. Harris, Stress-Intensity Factors for Surface Cracks in Pipes: A Computer Code for Evaluation by Use of Influence Functions, EPRI NP-2425, Electric Power Research Institute (June 1982).